Energies **2014**, *7*, 8446-8464; doi:10.3390/en7128446

OPEN ACCESS

energies

ISSN 1996-1073

www.mdpi.com/journal/energies

Article

Comparison Study on Two Model-Based Adaptive Algorithms for SOC Estimation of Lithium-Ion Batteries in Electric Vehicles

Yong Tian [1], Bizhong Xia [1,*], Mingwang Wang [2], Wei Sun [2] and Zhihui Xu [2]

[1] Division of Advanced Manufacturing, Graduate School at Shenzhen, Tsinghua University, Tsinghua Campus, the University Town, Shenzhen 518055, China; E-Mail: tian.yong@sz.tsinghua.edu.cn

[2] Sunwoda Electronic Co. Ltd., Yihe Road, Baoan District, Shenzhen 518108, China; E-Mails: wangmw@sunwoda.com (M.W.); sunwei@sunwoda.com (W.S.); luojie@sunwoda.com (Z.X.)

***** Author to whom correspondence should be addressed; E-Mail: xiabz@sz.tsinghua.edu.cn; Tel./Fax: +86-755-2603-6757.

External Editor: Izumi Taniguchi

Received: 22 August 2014; in revised form: 17 November 2014 / Accepted: 10 December 2014 / Published: 17 December 2014

Abstract: State of charge (SOC) estimation is essential to battery management systems in electric vehicles (EVs) to ensure the safe operations of batteries and providing drivers with the remaining range of the EVs. A number of estimation algorithms have been developed to get an accurate SOC value because the SOC cannot be directly measured with sensors and is closely related to various factors, such as ambient temperature, current rate and battery aging. In this paper, two model-based adaptive algorithms, including the adaptive unscented Kalman filter (AUKF) and adaptive slide mode observer (ASMO) are applied and compared in terms of convergence behavior, tracking accuracy, computational cost and estimation robustness against parameter uncertainties of the battery model in SOC estimation. Two typical driving cycles, including the Dynamic Stress Test (DST) and New European Driving Cycle (NEDC) are applied to evaluate the performance of the two algorithms. Comparison results show that the AUKF has merits in convergence ability and tracking accuracy with an accurate battery model, while the ASMO has lower computational cost and better estimation robustness against parameter uncertainties of the battery model.

Keywords: lithium-ion battery; state of charge; adaptive unscented Kalman filter; adaptive slide mode observer

---

1. Introduction

Electric vehicles (EVs) have rapidly developed in the past few years due to the increasing cost of energy and global warming constraints. A battery management system (BMS) is important for EVs to safeguard the battery performance and extend its life [1]. An accurate state of charge (SOC) estimation is the most key technique in a BMS, since it indicates the remaining energy in the battery, which is helpful to prevent the battery from over-charging or over-discharging, which may damage the battery. The simplest definition of SOC is the ratio between the remaining capacity of the battery and its nominal capacity. However, it is difficult to get an accurate value of SOC, because the SOC cannot be directly measured with sensors and is closely related to various factors, such as ambient temperature, current rate and battery aging.

Numerous SOC estimation approaches have been proposed with the development of EVs, and each with its own advantages and disadvantages. A most commonly used method in practice is the Ampere-hour (Ah) counting (or Coulomb counting) method [2,3]. The Ah method obtains the remaining capacity of a battery by integrating the current over the time. It is simple and can be easily implemented on-board, because it only needs to measure the battery operating current and does not need complex computations. However, this method can easily cause accumulated calculation errors due to uncertain disturbances in the current measurement process and a lack of correction for the initial SOC offset. The open-circuit voltage (OCV) method estimates the SOC according to the relationship between the OCV and the SOC [4,5]. Nevertheless, it is not suitable for online estimation due to the long rest time to reach the steady-state of the battery. Computational intelligence algorithms, such as artificial neural networks (ANNs) [6–8], fuzzy-logic [9–11], and support vector machines (SVMs) [12,13] have also been developed to estimate the SOC. These methods do not require detailed knowledge of the battery systems, thus, they can be applied to all battery types and have excellent estimation performance if the training data is sufficient to cover all loading conditions. However, it is time consuming and nearly impossible to collect training data that can cover all possible loading conditions. Besides, all the aforementioned methods are open-loop estimation algorithms and do not require the battery model.

Additional efforts have been focused on model-based and closed-loop estimation methods, including the Kalman filter (KF) [14–38] and sliding mode observer (SMO) [39–43]. Despite requiring a higher computation cost than the A ħ method, these methods have merits in being self-correcting and involving online computing as well as the availability of the dynamic SOC estimation error range. Thus, they are increasingly popular and more suitable for real-time application than the other types of SOC estimation methods. To expand the application of KF in nonlinear battery systems, the Extended KF (EKF) and Unscented KF (UKF) have been developed. The EKF-based methods have been widely used for battery SOC estimation [14–27]. However, the application of EKF in practice has some shortcomings. For example, the linearizing process causes large linearization errors and complicated computation of the Jacobian matrix that may lead to instability of the filter and inaccurate estimation for highly nonlinear battery systems [30]. The UKF has been demonstrated to have a higher accuracy in estimating the mean and the error covariance of the state vector than EKF, and it does not need the complicated computation of the Jacobian matrix [28–38]. On the other hand, in KF algorithms, the process and measurement noise covariances are critical for the filtering performance and stability. In both EKF and UKF, constant values of the process and measurement noise covariances usually need to be pre-specified by a trial-and-error

method which is time consuming, laborious and error-prone [30]. Too small values of the process noise covariance and/or the measurement noise covariance at the beginning of the estimation process may result in a tight uncertainty tube around the true value and a biased solution, while too large values may lead to filter divergence [44]. For the battery SOC estimation, inappropriate values of the noise covariances will cause large estimation errors. Therefore, an adaptive unscented Kalman filter (AUKF) was developed in [30] to improve the SOC estimation accuracy by adaptively updating the process and measurement noise covariances based on the output voltage residual sequence of the battery model.

More recently, the SMO-based SOC estimation approaches have been developed to handle the battery model uncertainties, external disturbances and measurement noises [39–42]. Nevertheless, these methods rely on details about the battery dynamics for the appropriate selection of SMO parameters, such as uncertainty boundaries and switching gains, which may lead to the trade-off between the chattering magnitude and the convergence speed in the SOC estimation [43]. To overcome such a problem, an adaptive sliding mode observer (ASMO) for the SOC estimation has been proposed in [43]. Compared with the traditional SMO, the ASMO is able to dynamically adjust the switching gains in response to the tracking errors, and guarantee the reachability of sliding mode surface and trigger the sliding mode, thereby improving the SOC estimation accuracy.

In this paper, a comparison study between the two model-based adaptive algorithms above is carried out using the experimental data collected from a lithium-ion battery test bench. Two typical driving cycles, namely the Dynamic Stress Test (DST) and New European Driving Cycle (NEDC) are used to evaluate the performance of the algorithms in terms of convergence behavior, tracking accuracy, computational cost and estimation robustness against parameter uncertainties.

The remainder of the paper is organized as follows: in Section 2, the battery state functions are established based on an equivalent circuit model which is used to characterize the dynamic behaviors of the lithium-ion battery, and the method for battery model parameter identification is discussed. Section 3 introduces the principles of AUKF- and ASMO-based SOC estimation algorithms in detail. Section 4 presents the experimental results and discussion, and Section 5 provides the conclusions of the paper.

2. Battery Modeling and Parameter Identification

2.1. Battery Equivalent Circuit Model

Both the UKF and SMO are model-based methods, so precise battery models are required to accurately estimate the SOC values. Numerous models have been developed to simulate the dynamic characteristics of batteries. The equivalent circuit models (ECMs) with lumped parameters have been widely used in SOC estimation applications due to their good performance in describing the dynamic voltage characteristics of a lithium-ion battery [1,44]. The most common ECMs are comprised of resistor and resistor-capacitor (RC) network(s) connected in series. Based on the conclusion that adding RC networks can increase the model accuracy, but adding more complexity beyond two RC networks is not helpful [44], this paper selects the second-order RC model to establish the state functions for battery SOC estimation. As shown in Figure 1, the second-order RC battery equivalent circuit model consists of an open-circuit voltage U_{oc}(SOC), a resistor R_o, and two RC networks connected in series. The resistor R_o represents the ohmic resistance caused by the accumulation and dissipation of charge in the electrical

double-layer, R_{p1} and C_{p1} are the activation polarization resistance and capacitance respectively, R_{p2} and C_{p2} respectively are the concentration polarization resistance and capacitance.

Figure 1. Schematic diagram of the second-order RC battery equivalent circuit model.

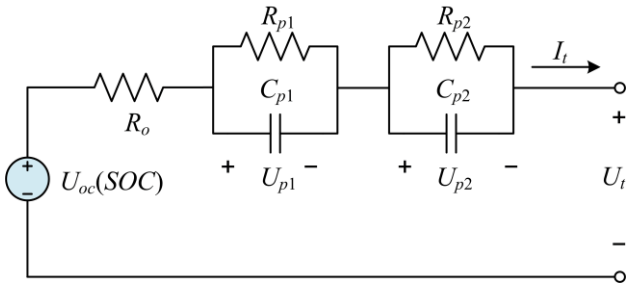

According to the circuit theory, the electrical behavior of the second-order RC battery equivalent circuit model shown in Figure 1 can be derived as:

$$\begin{cases} \dot{SOC} = -\dfrac{1}{C_n} I_t + v_1 \\ \dot{U}_{p1} = -\dfrac{1}{R_{p1}C_{p1}} U_{p1} + \dfrac{1}{C_{p1}} I_t + v_2 \\ \dot{U}_{p2} = -\dfrac{1}{R_{p2}C_{p2}} U_{p2} + \dfrac{1}{C_{p2}} I_t + v_3 \end{cases} \tag{1}$$

$$U_t = U_{oc}(\mathrm{SOC}) - U_{p1} - U_{p2} - R_o I_b + w \tag{2}$$

where C_n is the battery nominal capacity; U_{p1} and U_{p2} are the terminal voltage of C_{p1} and C_{p2}, respectively; U_t and I_t are the battery terminal voltage and current, respectively; U_{oc} represents the open circuit voltage (OCV) which is related to the values of SOC; v_1, v_2, v_3 and w represent noises caused by model uncertainties and external disturbances.

By selecting $x = (SOC, U_{p1}, U_{p2})^T$ as the state vector, and considering the current I_t and voltage U_t as the model input and output respectively, the discrete-time state equations of the second-order RC battery equivalent circuit model can be obtained as:

$$x_k = f(x_{k-1}, u_k) + w_k \tag{3}$$

$$y_k = h(x_k, u_k) + v_k \tag{4}$$

where f and h are the nonlinear process and measurement functions, respectively; x_k represents the unmeasurable state vector at time step k; u_k ($=I_{t,k}$) stands for the input vector; y_k ($=U_{t,k}$) is the observed output; v_k ($=(v_{1,k}\ v_{2,k}\ v_{3,k})^T$) and w_k are separately the process and measurement noises, which are both uncorrelated zero-mean Gaussian white sequences.

2.2. Battery Model Parameters Identification

In order to estimate the battery SOC based on the second-order RC battery equivalent circuit model, the model parameters, including the OCV-SOC relationship, R_o, R_{p1}, C_{p1}, R_{p2} and C_{p2} need to be determined. In order to acquire the data used to determine the relationship of OCV *vs.* SOC, a pulse

discharge experiment was carried out based on an ICR18650-22F type lithium-ion battery. More details about the battery parameters and the test bench configurations will be provided in Section 4. The test procedure is summarized as follows [45]: (1) The battery is fully charged at room temperature using the standard charging method, and then it is left in the open-circuit condition for 5 h; (2) the battery terminal voltage is measured and the measured voltage is regarded as the equilibrium potential since the battery is assumed to have reached the steady state; (3) the battery is discharged with a constant current of 0.1C A by 10% of the nominal capacity, and then it is left in the open-circuit condition for 2 h; (4) steps (2) and (3) are repeatedly performed until the battery is fully discharged. The measured data and the fitted curves with different broken-lines, including four-stage broken-line (4-broken-line) and ten-stage broken-line (10-broken-line) are shown in Figure 2. Despite the fact that the OCV-SOC curves of lithium-ion batteries are nonlinear, there exists a piecewise linear relationship between the OCV and the SOC in a certain range of SOC [43] indicated by the red circles in Figure 2. Therefore, in this paper the broken-lines are used to reduce the complexity of the OCV-SOC function.

Figure 2. Experimental OCV-SOC relationship of a lithium-ion battery.

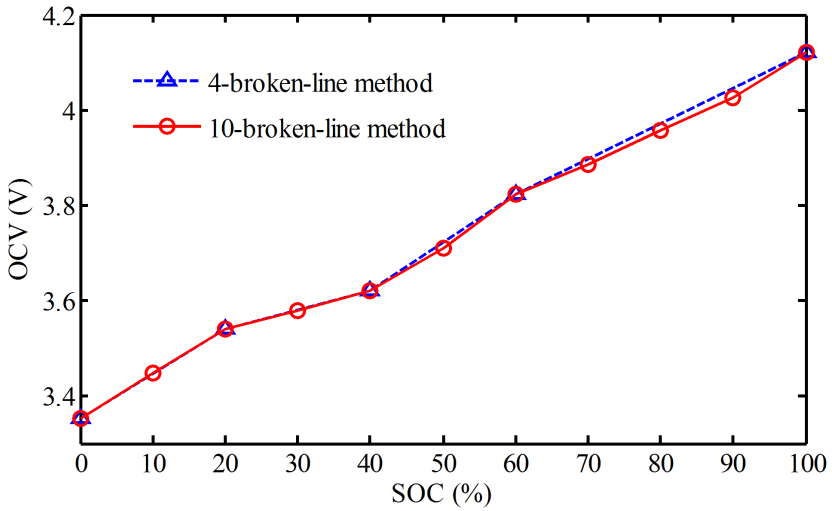

The exponential-function fitting method [43] was applied to determine the other parameters of the battery model in Figure 1 (e.g., R_o, R_{p1}, C_{p1}, R_{p2} and C_{p2}) based on the transient response of terminal voltage by executing a pulse-current discharging process at the room temperature [45]. The identified parameters are summarized in Table 1.

Table 1. Identified parameters of the second-order RC battery equivalent circuit model.

R_o	R_{p1}	C_{p1}	R_{p2}	C_{p2}
0.0344 Ω	0.0191 Ω	1513 F	0.0077 Ω	15428 F

3. AUKF and ASMO Algorithms for SOC Estimation

3.1. AUKF Algorithm

The adaptive unscented Kalman filter (AUKF) can adaptively update the process and measurement noise covariances based on the output voltage residual sequence of the battery model [30]. Thus,

it addresses the issue of the standard EKF and UKF that inappropriate values of the noise covariances cause large error. The process of the AUKF can be summarized as follows [30]:

(1) Initialization:

(a) Initial a posteriori error covariance: P_0;
(b) Initial process noise covariance: Q_0;
(c) Initial measurement noise covariance: V_0;
(d) Window size for covariance matching: L_w;
(e) Initial mean $\overline{x}_0$ and covariance P_0 with a random state vector x_0 as follows:

$$\overline{x}_0 = E[x_0] \tag{5}$$

$$P_0 = E[(x_0 - \overline{x}_0)(x_0 - \overline{x}_0)^T] \tag{6}$$

(2) Generate sigma points at time step $k-1$:

$$\hat{\chi}_{k-1}^{[0]} = \hat{x}_{k-1} \tag{7}$$

$$\hat{\chi}_{k-1}^{[i]} = \hat{x}_{k-1} + \left(\sqrt{(N+\lambda)P_{k-1}}\right)_i \quad i = 1, 2, \cdots, N \tag{8}$$

$$\hat{\chi}_{k-1}^{[N+i]} = \hat{x}_{k-1} - \left(\sqrt{(N+\lambda)P_{k-1}}\right)_i \quad i = 1, 2, \cdots, N \tag{9}$$

where λ is a composite coefficient satisfying the following equation:

$$\lambda = \alpha^2(N + \kappa) - N \tag{10}$$

where N is the dimension of the state vector, α and κ are scaling parameters. The parameter α ($0 \leq \alpha \leq 1$) determines the spread of the sigma points around the mean value, and it should ideally be a small number [46]. The condition $\kappa \geq 0$ should be satisfied to guarantee the semi-positive definiteness of the covariance matrix, and a good default choice is $\kappa = 0$ [47].

(3) Time update:

(a) Propagate sigma points through the process equation:

$$\hat{\chi}_k = f(\hat{\chi}_{k-1}, u_k) + w_k \tag{11}$$

(b) Calculate the mean of state variable:

$$\overline{x}_k = \sum_{i=0}^{2N} W_m^{[i]} \hat{\chi}_k^{[i]} \tag{12}$$

where $W_m^{[i]}$ are weights defined as:

$$W_m^{[0]} = \frac{\lambda}{N + \lambda} \tag{13}$$

$$W_m^{[i]} = \frac{1}{2(N+\lambda)} \quad i = 1, 2, \cdots, 2N \tag{14}$$

(c) Calculate the propagated covariance:

$$\hat{P}_{x,k} = \sum_{i=0}^{2N} W_c^{[i]} \left(\hat{\chi}_k^{[i]} - \overline{x}_k\right)\left(\hat{\chi}_k^{[i]} - \overline{x}_k\right)^T + Q_k \tag{15}$$

where Q_k is the process noise covariance matrix at time step k and weights $W_c^{[i]}$ is defined as:

$$W_c^{[0]} = \frac{\lambda}{N+\lambda} + (1-\alpha^2+\beta) \tag{16}$$

$$W_c^{[i]} = \frac{1}{2(N+\lambda)} \quad i = 1, 2, \cdots, 2N \tag{17}$$

where β is a nonnegative scaling factor used to incorporate prior knowledge of the distribution, and the optimal choice is β = 2 for a Gaussian distribution [41].

(4) Measurement update

(a) Propagate sigma points through the measurement equation:

$$\hat{y}_k = h(\hat{\chi}_k, u_k) + v_k \tag{18}$$

(b) Calculate the mean of output variable:

$$\overline{y}_k = \sum_{i=0}^{2N} W_m^{[i]} \hat{y}_k^{[i]} \tag{19}$$

(c) Calculate the estimated covariance:

$$\hat{P}_{y,k} = \sum_{i=0}^{2N} W_c^{[i]} \left(\hat{y}_k^{[i]} - \overline{y}_k \right) \left(\hat{y}_k^{[i]} - \overline{y}_k \right)^T + V_k \tag{20}$$

$$\hat{P}_{xy,k} = \sum_{i=0}^{2N} W_c^{[i]} \left(\hat{\chi}_k^{[i]} - \overline{x}_k \right) \left(\hat{y}_k^{[i]} - \overline{y}_k \right)^T \tag{21}$$

where V_k is the measurement noise covariance matrix at time step k.

(5) Measurement correction

(a) Calculate the Kalman gain:

$$K_k = \hat{P}_{xy,k} \hat{P}_{y,k}^{-1} \tag{22}$$

(b) Update the estimated state:

$$\hat{x}_k = \overline{x}_k + K_k \left(y_k - \overline{y}_k \right) \tag{23}$$

(c) Update the propagated covariance:

$$P_k = \hat{P}_{x,k} - K_k \hat{P}_{y,k} K_k^T \tag{24}$$

(6) Adjustment of Q_k and V_k

$$\begin{cases} Q_k = K_k F_k K_k^T \\ V_k = F_k + \sum_{i=0}^{2N} W_c^{[i]} \left(\hat{y}_k^{[i]} - \overline{y}_k \right) \left(\hat{y}_k^{[i]} - \overline{y}_k \right)^T \end{cases} \tag{25}$$

where F_k is an approximation to the covariance of the voltage residual at time step k and is defined as:

$$F_k = \sum_{i=k-L_w+1}^{k} e_i e_i^T \tag{26}$$

where e_i is the voltage residual of the battery model at time step i, and L_w is window size for covariance matching. More details about the AUKF algorithm can be found in [30] and [34].

3.2. ASMO Algorithm

With the piecewise linearisation method shown in Figure 2, the OCV-SOC relationship can be formulated as:

$$U_{oc}(SOC) = k_1 SOC + k_2 \tag{27}$$

where the values of k_1 and k_2 are varying in different SOC ranges, and their values can be obtained with linear fitting method in different SOC ranges as shown in Figure 2.

Due to the fast sampling rate [43], the changing rate of discharge current I_t can be negligible, that's to say, $dI_t/dt = 0$. Thus, the time derivative of terminal voltage U_t in Equation (2) with the substitutions of Equations (1) and (27) can be obtained as:

$$\dot{U}_t = -\frac{I_t}{C_n}k_1 + \frac{1}{R_{p1}C_{p1}}U_{p1} - \frac{1}{C_{p1}}I_t + \frac{1}{R_{p2}C_{p2}}U_{p2} - \frac{1}{C_{p2}}I_t + w \tag{28}$$

By solving I_t in Equation (2) and substituting it into Equation (1) as well as rearranging Equations (1) and (28), the state-space equations of the second-oder RC battery equivalent circuit model can be derived as:

$$\begin{cases} \dot{U}_t = -a_1 U_t + a_1 U_{oc}(SOC) - a_3 U_{p1} - a_4 U_{p2} - b_1 I_t + w \\ S\dot{O}C = a_2 U_t - a_2 U_{oc}(SOC) + a_2 U_{p1} + a_2 U_{p2} + v_1 \\ \dot{U}_{p1} = -a_3 U_{p1} + b_2 I_t + v_2 \\ \dot{U}_{p2} = -a_4 U_{p2} + b_3 I_t + v_3 \end{cases} \tag{29}$$

where $a_1 = 1/(R_{p1}C_{p1} + 1/(R_{p2}C_{p2}))$, $a_2 = 1/(R_oC_n)$, $a_3 = 1/(R_{p1}C_{p1})$, $a_4 = 1/(R_{p2}C_{p2})$, $b_1 = k_1/C_n + R_o/(R_{p1}C_{p1}) + 1/C_{p1} + R_o/(R_{p2}C_{p2}) + 1/C_{p2}$, $b_2 = 1/C_{p1}$ and $b_3 = 1/C_{p2}$.

By selecting $x = [U_t\ U_{oc}\ U_{p1}\ U_{p2}]^T$ as the state vector, and considering the model input and output as $u = I_t$ and $y = U_t$, respectively, the discrete-time state equations of the second-order RC battery equivalent circuit model can be concisely expressed in matrices as follows:

$$x_k = Ax_{k-1} + Bu_k + \Gamma\xi_k \tag{30}$$

$$y_k = Cx_k \tag{31}$$

where $\Gamma\xi_k$ represents modeling errors and random disturbances at time step k. The parameter Γ is the uncertainty input matrix. The parameter ξ_k is assumed to be bounded $|\xi_k| \le h_0$, in which h_0 is a constant. The matrices A, B and C are given as: $A = \begin{bmatrix} -a_1 & a_1 & -a_3 & -a_4 \\ a_2 & -a_2 & a_2 & a_2 \\ 0 & 0 & -a_3 & 0 \\ 0 & 0 & 0 & -a_4 \end{bmatrix}$, $B = \begin{bmatrix} -b_1 \\ 0 \\ b_2 \\ b_3 \end{bmatrix}$, $\xi_k = \begin{bmatrix} w_k \\ v_{1,k} \\ v_{2,k} \\ v_{3,k} \end{bmatrix}$ and $C = \begin{bmatrix} 1 & 0 & 0 & 0 \end{bmatrix}$.

The adaptive sliding mode observer for the system in Equations (30) and (31) is designed as:

$$\hat{x}_k = A\hat{x}_{k-1} + Bu_k + He_{y,k} + \rho\Gamma \operatorname{sgn}(e_{y,k}) \tag{32}$$

$$\hat{y}_k = C\hat{x}_k \tag{33}$$

where $e_{y,k} = y_k - \hat{y}_k$ is the observation error, H is the feedback gain matrix, ρ is the adaptive switching gains function which can be designed to guarantee the stability and robustness of the AGMO as follows:

$$\rho = \begin{cases} \sigma \left| e_{y,k} \right| & if\ e_{y,k} \neq 0 \\ 0 & if\ e_{y,k} = 0 \end{cases} \tag{34}$$

where σ is a positive constant used to adjust the speed adaptation for switching gains function.

The discontinuous switching term in Equation (32) is defined as:

$$\operatorname{sgn}(e_{y,k}) = \begin{cases} +1, & e_{y,k} > 0 \\ -1, & e_{y,k} < 0 \end{cases} \tag{35}$$

The feedforward gain matrix H can be obtained by using either the pole assignment method or linear quadratic regulator (LQR) method [39,43]. The LQR method is easier to obtain gain matrix H using the Riccati equation as:

$$AP + PA^T - PC^T R_H^{-1} CP = -Q_H \tag{36}$$

where Q_H and R_H respectively are arbitrary semi-positive definite and positive definite matrices, having a positive definite solution P. Then $A^T - C^T H^T$ is stable with:

$$H^T = R_H^{-1} CP \tag{37}$$

which is equivalent to the stability of $A - HC$ [39].

With appropriate Lyapunov equation, a matrix W is selected such that the reconstruction error system is asymptotically stable. By selecting an appropriate Lyapunov equation, there exists a symmetric definite matrix P_f as the solution of the Lyapunov equation:

$$(A - HC)P_f + P_f (A - HC)^T = -Q_f \tag{38}$$

where Q_f is an arbitrary positive definite matrix such that the structural constraint in Equation (39) can be guaranteed if W is a positive definite matrix:

$$\Gamma^T P_f = WC \tag{39}$$

More details about the error convergence proof of the SMO can be found in [39–43].

4. Evaluation and Discussion

4.1. Evaluation Method

A battery test bench, as shown in Figure 3, is established for the comparison study of the AUKF and ASMO-based SOC estimation approaches. The ICR18650-22F-type lithium-ion battery manufactured by Samsung SDI (Seoul, Korea) was used in the test. This kind of battery has a nominal voltage of 3.62 V and a nominal capacity of 2.2 A ħ. The electronic switch is applied to discharge the battery with the programmable electric load or charge it with the programmable power supply. The BMS

module is adopted to measure the battery voltage and current, transmit them to the host computer and send the control command to the switch through the CAN communication unit. The host computer is used to be an estimator computing the SOC values. The SOC values with the AUKF and ASMO algorithms are estimated in the Matlab software based on the measured battery voltage and current from the test bench, and compared with that obtained by the Coulomb counting method.

Figure 3. Schematic diagram of the test bench.

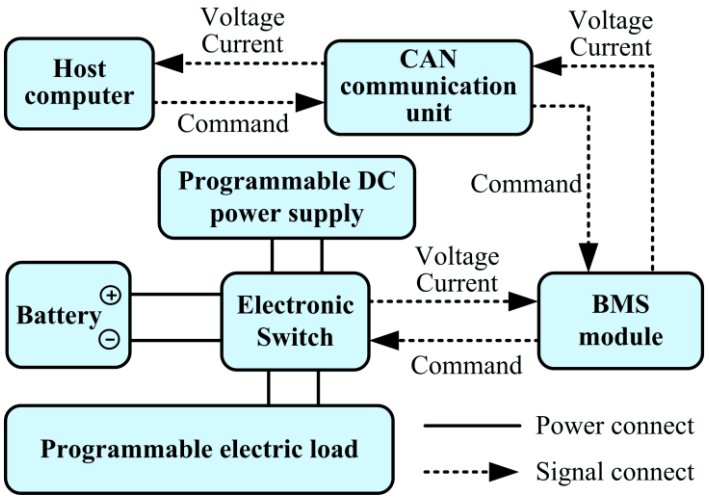

Two driving cycles, including the 360 s Dynamic Stress Test (DST) cycle and the 1184 s New European Driving Cycle (NEDC) [26,32] are utilized to evaluate the performance of SOC estimation approaches under the typical loading conditions when the EVs are on road. The current profiles under the DST and NEDC tests are shown in Figures 4 and 5 [45], respectively. Figure 4a and Figure 5a show the complete profiles *vs.* time, while Figure 4b and Figure 5b show the profiles of a single driving cycle.

Figure 4. Current profiles under DST test. (**a**) current *vs.* time profile; (**b**) a DST cycle.

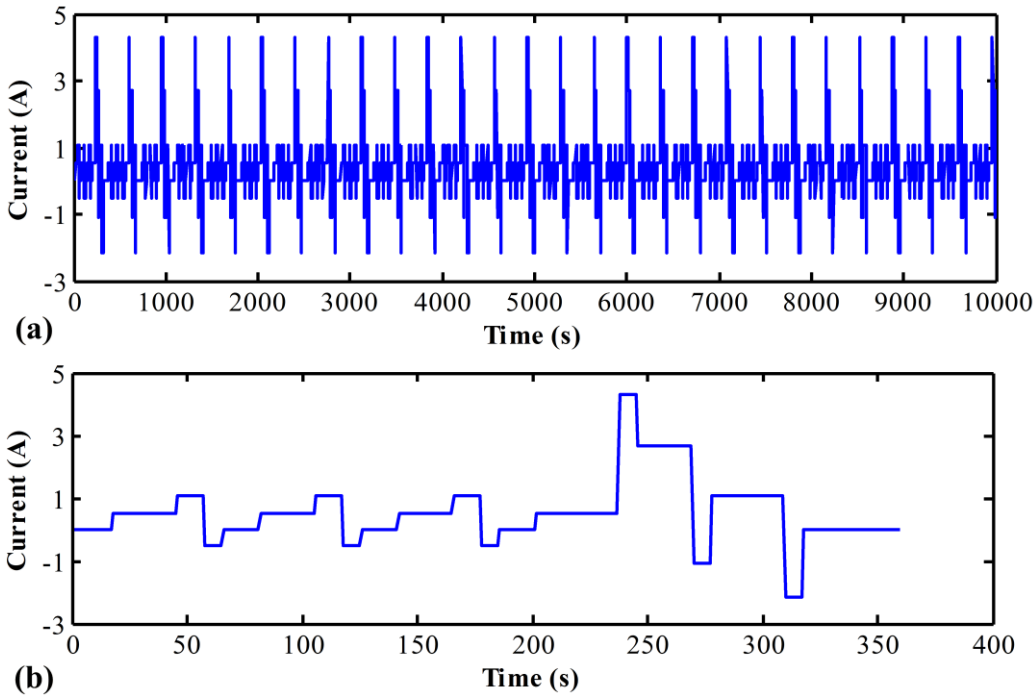

Figure 5. Current profiles under NEDC test. (**a**) current *vs.* time profile; (**b**) a NEDC cycle.

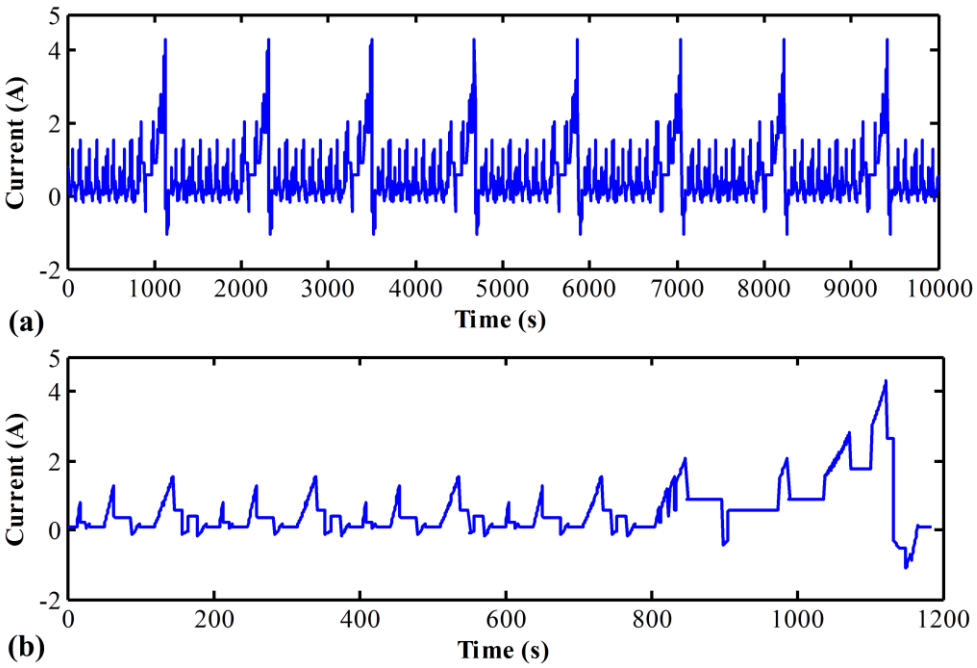

In this study, four aspects, including the convergence behavior, tracking accuracy, computational cost and estimation robustness against parameter uncertainties of the battery model are compared. In order to evaluate the robustness against parameter uncertainties, different values of ohmic resistance and OCV-SOC functions in Figure 2 are applied.

4.2. Comparison Results and Discussion

4.2.1. Estimation Results with Different Initial SOCs

To compare the convergence behavior of the AUKF and ASMO algorithms, the convergence rate to ±5% error bound with different initial SOCs from 0% to 100% in 10% steps under the DST and NEDC tests is obtained, and the results are shown in Tables 2 and 3, respectively. In addition, the corresponding root mean square errors (RMSEs) of SOC are summarized in Tables 4 and 5. As an example, the SOC estimation results with an initial SOC of 50% are shown in Figures 6 and 7. With all the results, it can be seen that two algorithms both can quickly track the reference SOC values with different initial SOCs, while the AUKF performs better with a faster convergence ability and a higher accuracy. Besides, the computational cost of AUKF algorithm obtained by the Maltab commands, including *tic* and *toc* is about 0.145 ms/point, while the value of ASMO algorithm is about 0.064 ms/point. Therefore, the ASMO performs better in terms of reducing computational cost and as a result, it can be more easily implemented in hardware. It is important to note that in this section the OCV-SOC relationship is fitted with the ten-stage broken-line as shown in Figure 2.

Table 2. Comparison of convergence rate (s) with different intial SOCs under DST test.

Initial SOC (%)	0	10	20	30	40	50	60	70	80	90	100
AUKF	388	361	337	319	313	300	277	187	82	7	0
ASMO	500	482	477	457	420	380	311	274	197	94	0

Table 3. Comparison of convergence rate (s) with different intial SOCs under NEDC test.

Initial SOC (%)	0	10	20	30	40	50	60	70	80	90	100
AUKF	359	342	315	306	287	280	250	186	84	7	0
ASMO	482	468	458	423	386	355	305	271	196	92	0

Table 4. Comparison of RMSEs (%) with different intial SOCs under DST test.

Initial SOC (%)	0	10	20	30	40	50	60	70	80	90	100
AUKF	1.396	1.323	1.248	1.171	1.066	0.965	0.864	0.738	0.590	0.486	0.463
ASMO	2.744	2.569	2.389	2.220	2.061	1.901	1.728	1.560	1.399	2.252	1.121

Table 5. Comparison of RMSEs (%) with different intial SOCs under NEDC test.

Initial SOC (%)	0	10	20	30	40	50	60	70	80	90	100
AUKF	1.362	1.291	1.218	1.144	1.042	0.944	0.844	0.720	0.579	0.481	0.459
ASMO	2.687	2.513	2.335	2.167	2.010	1.851	1.681	1.513	1.353	1.206	1.085

Figure 6. Comparison of SOC estimation with an initial SOC of 50% under DST test. (**a**) SOC; (**b**) SOC error.

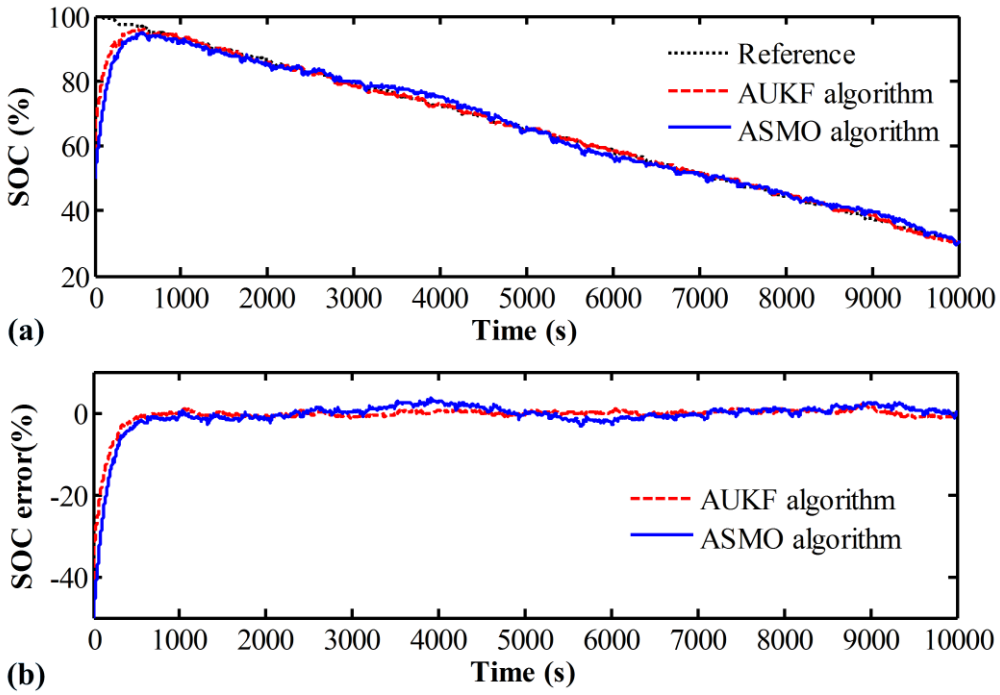

Figure 7. Comparison of SOC estimation with an initial SOC of 50% under NEDC test. (**a**) SOC; (**b**) SOC error.

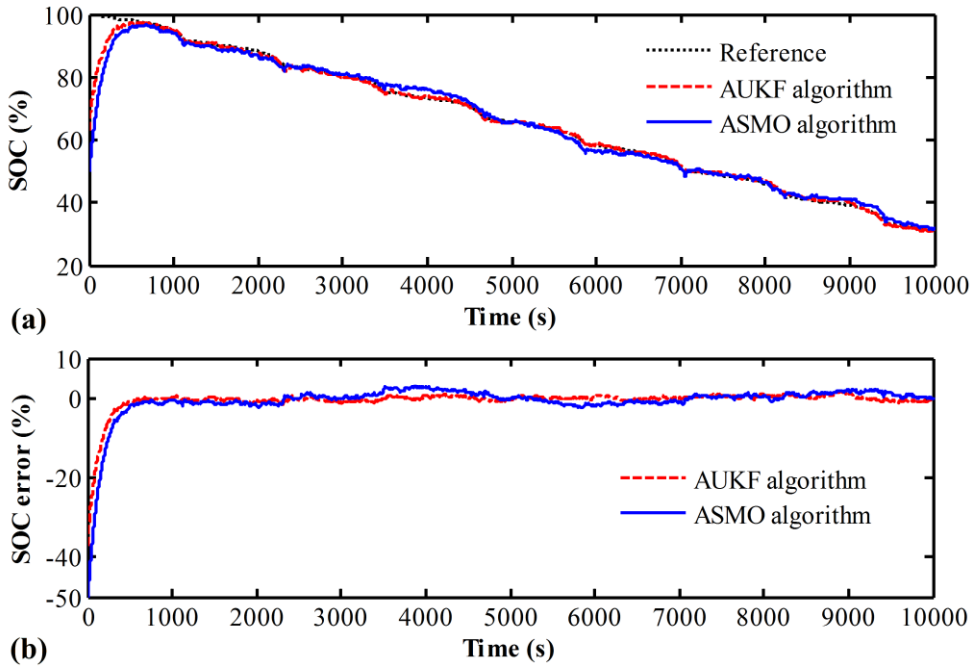

4.2.2. Estimation Results with Different Modeling Errors

The battery model parameters, including ohmic resistance, polarization resistance and capacitance as well as the OCV vary with various factors, such as the current rate, SOC, cycle number (battery aging) and operating temperature [35]. Besides, an accurate expression of relationship between the OCV and the SOC is crucial to improve the SOC estimation accuracy [48]. Therefore, in this section, different ohmic resistance values and different OCV-SOC functions are selected to be examples for comparing the robustness of AUKF and ASMO-based estimation approaches against the parameter uncertainties of the battery model. The values of ohmic resistance are set to be changed in the range of 0.2 R_o to 2.0 R_o with a step of 0.2 R_o to simulate the effect of different conditions, including current, SOC, aging and temperature on the ohmic resistance. Figure 8 shows the comparison results of SOC estimation with different ohmic resistance under the DST test, while Figure 9 shows them under the NEDC test. It is clearly indicated that although the AUKF algorithm, in most cases, has a higher accuracy with a lower mean absolute error (MAE), it has a poorer robusness againt the ohmic resistance uncertainty because its accuracy varies much more with the variation of ohmic resistance. Besides, the estimation accuracy of both the AUKF and ASMO algorithms decreases with the increase of ohmic resistance error.

In order to evaluate the robustness against OCV errors, two OCV-SOC functions shown in Figure 2, namely four-stage and ten-stage broken-lines are applied, and the values of k_1 and k_2 are shown in Tables 6 and 7, respectively. As an example, the AUKF and ASMO-based SOC estimation results with different OCV-SOC functions under NEDC test are shown in Figures 10 and 11, respectively. From Figures 10 and 11, it can be seen that the estimation error of AUKF algorithm highly increases with the decrease of OCV-SOC relationship accuracy, while that of ASMO algorithm slightly changes with the variation of OCV-SOC relationship accuracy. Therefore, it is concluded that the ASMO algorithm has a better robustness against the OCV errors.

Figure 8. Comparison of SOC estimation with different ohmic resistance under DST test. (**a**) MAE; (**b**) Max error.

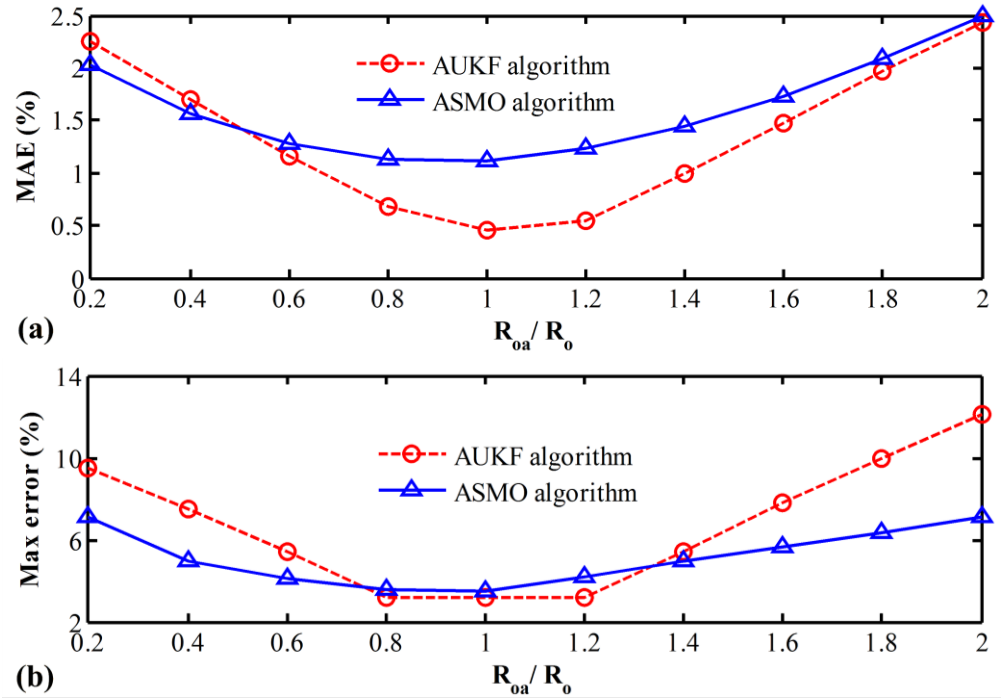

Figure 9. Comparison of SOC estimation with different ohmic resistance under NEDC test. (**a**) MAE; (**b**) Max error.

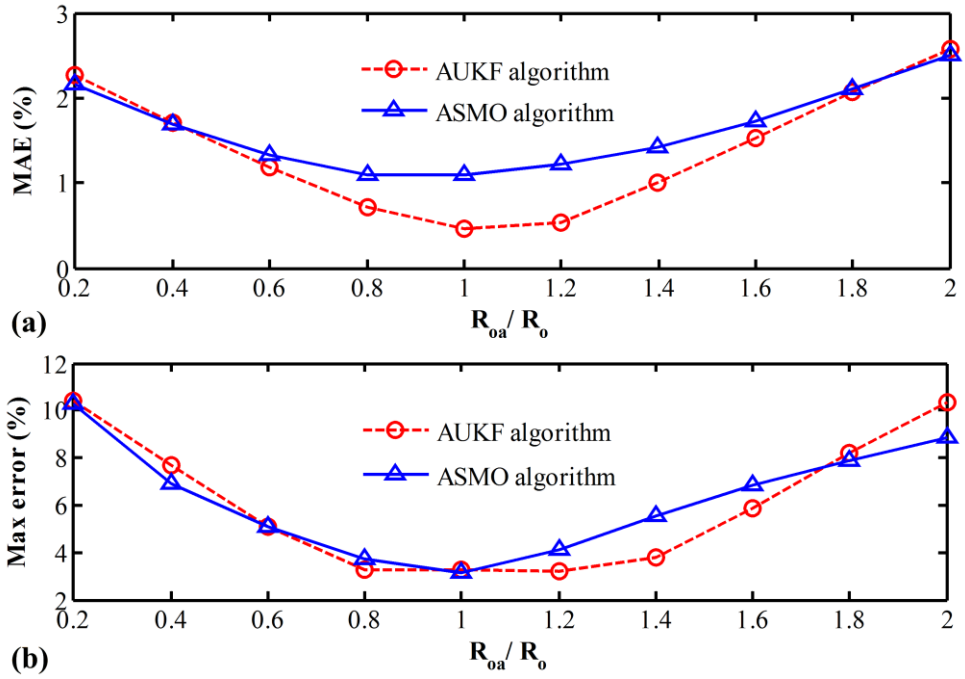

Table 6. Values of k_1 and k_2 with four-stage broken-lines.

SOC range (%)	0–20	20–40	40–60	60–100
k_1	0.940	0.395	1.020	0.737
k_2	3.353	3.461	3.207	3.373

Table 7. Values of k_1 and k_2 with ten-stage broken-lines.

SOC range (%)	0–10	10–20	20–30	30–40	40–50	50–60	60–70	70–80	80–90	90–100
k_1	0.970	0.910	0.380	0.410	0.900	1.140	0.630	0.710	0.680	0.970
k_2	3.352	3.358	3.464	3.455	3.259	3.139	3.445	3.389	3.413	3.152

Figure 10. AUKF-based SOC estimation with different OCV-SOC functions under NEDC test. (**a**) SOC; (**b**) SOC error.

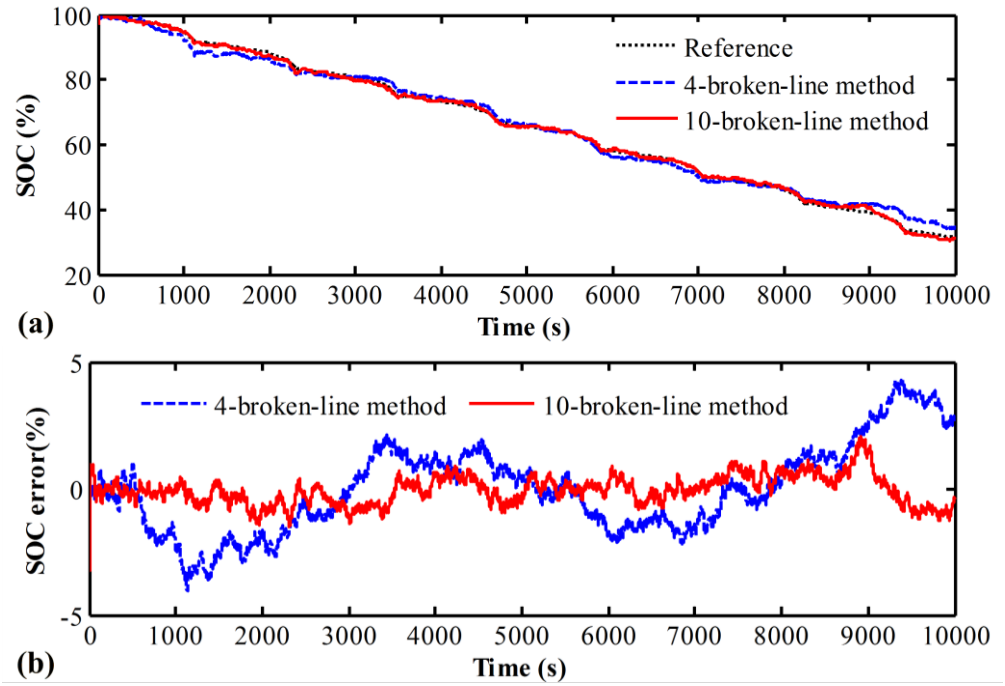

Figure 11. ASMO-based SOC estimation with different OCV-SOC functions under NEDC test. (**a**) SOC; (**b**) SOC error.

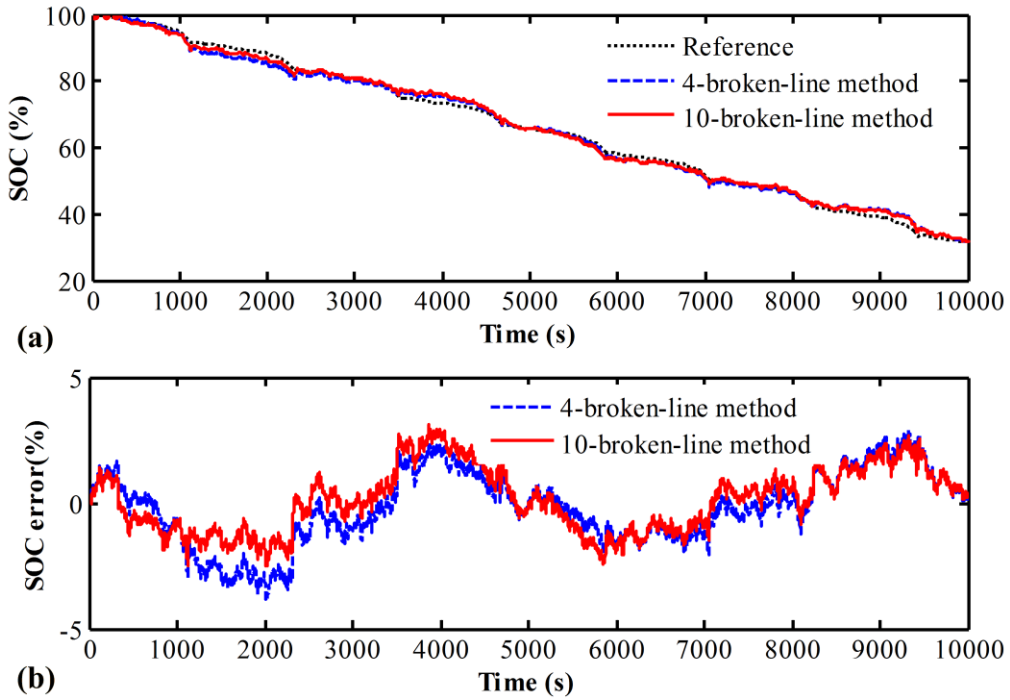

5. Conclusions

In this paper, two model-based adaptive algorithms, namely AUKF and ASMO, are applied to estimate the SOC of lithium-ion batteries in EVs and compared in terms of convergence ability, tracking accuracy, computational cost and estimation robustness. Firstly, the battery state equations are derived from the second-order RC battery equivalent circuit model, and the model parameters are identified with the exponential-function fitting method based on the data collected from a battery test bench. Then, the general formulations of AUKF and ASMO-based estimation approaches are studied. Finally, experiments based on the DST and NEDC cycles are carried out to evaluate the performance of estimation algorithms. Comparison results indicate that both the algorithms can deal well with the issues related to the initial SOC errors and modeling errors, but the AUKF performs better with a higher tracking accuracy and a faster convergence rate related to the initial SOC values. However, the ASMO has a lower computational cost and a better robustness against the parameter uncertainties of the battery model, such as different ohmic resistance values and different OCV-SOC functions.

Acknowledgments

This work was simultaneously supported by the China Postdoctoral Science Foundation Funded Project (No. 2013M540941) and the Shenzhen Key Laboratory of LED Packaging Funded Project (No. NZDSY20120619141243215).

Author Contributions

Yong Tian developed the essential idea behind the present research and prepared the manuscript at early stages. Mingwang Wang, Wei Sun and Zhihui Xu established the test bench and carried out the experiments. Final review, including final manuscript corrections, was done by Bizhong Xia and Yong Tian.

Conflicts of Interest

The authors declare no conflict of interest.

References

1. He, H.W.; Xiong, R.; Guo, H.Q.; Li, S.C. Comparison study on the battery models used for the energy management of batteries in electric vehicles. *Energy Convers. Manag.* **2012**, *64*, 113–121.
2. Aylor, J.H.; Thieme, A.; Johnson, B.W. A battery state-of-charge indicator for electric wheelchairs. *IEEE Trans. Ind. Electron.* **1992**, *39*, 398–409.
3. Ng, K.S.; Moo, C.S.; Chen, Y.P.; Hsieh, Y.C. Enhanced coulomb counting method for estimating state-of-charge and state-of-health of lithium-ion batteries. *Appl. Energy* **2009**, *86*, 1506–1511.
4. Pop, V.; Bergveld, H.J.; Notten, P.H.L.; Regtien, P.P.L. State-of-the-art of battery state-of-charge determination. *Meas. Sci. Technol.* **2005**, *16*, R93–R110.
5. Lee, S.; Kim, J.; Lee, J.; Cho, B.H. State-of-charge and capacity estimation of lithium-ion battery using a new open-circuit voltage *versus* state-of-charge. *J. Power Sources* **2008**, *185*, 1367–1373.

6. Shen, Y.Q. Adaptive online state-of-charge determination based on neuro-controller and neural network. *Energy Convers. Manag.* **2010**, *51*, 1093–1098.
7. Cheng, B.; Bai, Z.F.; Gao, B.G. State of charge estimation based on evolutionary neural network. *Energy Convers. Manag.* **2008**, *49*, 2788–2794.
8. Charkhgard, M.; Farrokhi, M. State-of-charge estimation for lithium-ion batteries using neural networks and EKF. *IEEE Trans. Ind. Electron.* **2010**, *57*, 4178–4187.
9. Salkind, A.J.; Fennie, C.; Singh, P.; Atwater, T.; Reisne, D.E. Determination of state-of-charge and state-of-health of batteries by fuzzy logic methodology. *J. Power Sources* **1999**, *80*, 293–300.
10. Singh, P.; Vinjamuri, R.R.; Wang, X.Q.; Reisner, D. Design and implementation of a fuzzy logic-based state-of-charge meter for li-ion batteries used in portable defibrillators. *J. Power Sources* **2006**, *162*, 829–836.
11. Malkhandi, S. Fuzzy logic-based learning system and estimation of state of charge of lead-acid battery. *Eng. Appl. Artif. Intell.* **2006**, *19*, 479–485.
12. Hansen, T.; Wang, C.J. Support vector based battery state of charge estimator. *J. Power Sources* **2005**, *141*, 351–358.
13. Shi, Q.; Zhang, C.; Cui, N. Estimation of battery state-of-charge using v-support vector regression algorithm. *Int. J. Autom. Technol.* **2008**, *9*, 759–764.
14. Plett, G.L. Extended Kalman filtering for battery management systems of LiPB-based HEV battery packs Part 1. Background. *J. Power Sources* **2004**, *134*, 252–261.
15. Plett, G.L. Extended Kalman filtering for battery management systems of LiPB-based HEV battery packs Part 2. Modeling and identification. *J. Power Sources* **2004**, *134*, 262–276.
16. Plett, G.L. Extended Kalman filtering for battery management systems of LiPB-based HEV battery packs Part 3. State and parameter estimation. *J. Power Sources* **2004**, *134*, 277–292.
17. Lee, J.; Nam, O.; Cho, B.H. Li-ion battery SOC estimation method based on the reduced order extended Kalman filtering. *J. Power Sources* **2007**, *174*, 9–15.
18. Yuan, S.F.; Wu, H.J.; Yin, C.L. State of charge estimation using the extended Kalman filter for battery management systems based on the ARX battery model. *Energies* **2013**, *6*, 444–470.
19. Hu, X.S.; Li, S.B.; Peng, H.; Sun, F.C. Robustness analysis of state-of-charge estimation methods for two types of Li-ion batteries. *J. Power Sources* **2012**, *217*, 209–219.
20. Dai, H.F.; Wei, X.Z.; Sun, Z.C.; Wang, J.Y.; Gu, W.J. Online cell SOC estimation of Li-ion battery packs using a dual time-scale Kalman filtering for EV applications. *Appl. Energy* **2012**, *95*, 227–237.
21. Hu, C.; Youn, B.D.; Chung, J. A multiscale framework with extended Kalman filter for lithium-ion battery SOC and capacity estimation. *Appl. Energy* **2012**, *92*, 694–704.
22. Wang, J.P.; Guo, J.G.; Ding, L. An adaptive Kalman filtering based State of Charge combined estimator for electric vehicle battery pack. *Energy Convers. Manag.* **2009**, *50*, 3182–3186.
23. Han, J.Y.; Kim, D.C.; Sunwoo, M. State-of-charge estimation of lead-acid batteries using an adaptive extended Kalman filter. *J. Power Sources* **2009**, *188*, 606–612.
24. Xiong, R.; Gong, X.Z.; Mi, C.C.; Sun, F.C. A robust state-of-charge estimator for multiple types of lithium-ion batteries using adaptive extended Kalman filter. *J. Power Sources* **2013**, *243*, 805–816.

25. Sepasi, S.; Ghorbani, R.; Liaw, B.Y. A novel on-board state-of-charge estimation method for aged Li-ion batteries based on model adaptive extended Kalman filter. *J. Power Sources* **2014**, *245*, 337–344.
26. Xiong, R.; He, H.W.; Sun, F.C.; Zhao, K. Evaluation on state of charge estimation of batteries with adaptive extended Kalman filter by experiment approach. *IEEE Trans. Veh. Technol.* **2013**, *62*, 108–117.
27. He, H.W.; Xiong, R.; Zhang, X.W.; Sun, F.C.; Fan, J.X. State-of-charge estimation of the lithium-ion battery using an adaptive extended Kalman filter based on an improved Thevenin model. *IEEE Trans. Veh. Technol.* **2011**, *60*, 1461–1469.
28. Plett, G.L. Sigma-point Kalman filtering for battery management systems of LiPB-based HEV battery packs Part 1: Introduction and state estimation. *J. Power Sources* **2006**, *161*, 1356–1368.
29. Plett, G.L. Sigma-point Kalman filtering for battery management systems of LiPB-based HEV battery packs-Part 1: Introduction and state estimation, Part 2: Simultaneous state and parameter estimation. *J. Power Sources* **2006**, *161*, 1369–1384.
30. Sun, F.C.; Hu, X.S.; Zou, Y.; Li, S.G. Adaptive unscented Kalman filtering for state of charge estimation of a lithium-ion battery for electric vehicles. *Energy* **2011**, *36*, 3531–3540.
31. He, Z.W.; Gao, M.Y.; Wang, C.S.; Wang, L.Y.; Liu, Y.Y. Adaptive state of charge estimation for Li-ion batteries based on an unscented Kalman filter with an enhanced battery model. *Energies* **2013**, *6*, 4134–4151.
32. Xing, Y.J.; He, W.; Pecht, M.; Tsui, K.L. State of charge estimation of lithium-ion batteries using the open-circuit voltage at various ambient temperatures. *Appl. Energy* **2014**, *113*, 106–115.
33. He, W.; Williard, N.; Chen, C.C.; Pecht, M. State of charge estimation for electric vehicle batteries using unscented Kalman filtering. *Microelectron. Reliab.* **2013**, *53*, 840–847.
34. Partovibakhsh, M.; Liu, G.J. An adaptive unscented Kalman filtering approach for online estimation of model parameters and state-of-charge of Lithium-ion batteries for autonomous mobile robots. *IEEE Trans. Control. Syst. Technol.* **2014**, doi:10.1109/TCST.2014.2317781.
35. Tian, Y.; Xia, B.Z.; Sun, W.; Xu, Z.H.; Zheng, W.W. A modified model based state of charge estimation of power lithium-ion batteries using unscented Kalman filter. *J. Power Sources* **2014**, *270*, 619–626.
36. Hu, X.S.; Sun, F.C.; Zou, Y. Comparison between two model-based algorithms for Li-ion battery SOC estimation in electric vehicles. *Simul. Model. Pract. Theory* **2013**, *34*, 1–11.
37. He, H.W.; Qin, H.Z.; Sun, X.K.; Shui, Y.P. Comparison study on the battery SoC estimation with EKF and UKF algorithms. *Energies* **2013**, *6*, 5088–5100.
38. Li, J.H.; Barillas, J.K.; Guenther, C.; Danzer, M.A. A comparative study of state of charge estimation algorithms for $LiFePO_4$ batteries used in electric vehicles. *J. Power Sources* **2013**, *230*, 244–250.
39. Kim, I.S. The novel state of charge estimation method for lithium battery using sliding mode observer. *J. Power Sources* **2006**, *163*, 584–590.
40. Chen, X.P.; Shen, W.X.; Cao, Z.W.; Kapoor, A.; Hijazin, I. Adaptive gain sliding mode observer for state of charge estimation based on combined battery equivalent circuit model in electric vehicles. In Proceedings of IEEE 8th Conference on Industrial Electronics and Applications, Melbourne, Australia, 19–21 June 2013; IEEE: Piscataway, NJ, USA, 2013; pp. 601–606.

41. Kim, D.; Koo, K.; Jeong, J.J.; Goh, T.; Kim, S.W. Second-order discrete-time sliding mode observer for state of charge determination based on a dynamic resistance Li-ion battery model. *Energies* **2013**, *6*, 5538–5551.
42. Kim, I.L.S. A technique for estimating the state of health of Lithium batteries through a dual-sliding-mode observer. *IEEE Trans. Power Electron.* **2010**, *25*, 1013–1022.
43. Chen, X.P.; Shen, W.X.; Gao, Z.W.; Kapoor, A. A novel approach for state of charge estimation based on adaptive switching gain sliding mode observer in electric vehicles. *J. Power Sources* **2014**, *246*, 667–678.
44. Hu, X.S.; Li, S.B.; Peng, H. A comparative study of equivalent circuit models for Li-ion batteries. *J. Power Sources* **2012**, *198*, 359–367.
45. Tian, Y.; Chen, C.R.; Xia, B.Z.; Sun, W.; Xu, Z.H.; Zheng, W.W. An adaptive gain nonlinear observer for state of charge estimation of lithium-ion batteries in electric vehicles. *Energies* **2014**, *7*, 5995–6012.
46. Mohamed, A.H.; Schwarz, K.P. Adaptive Kalman filtering for INS/GPS. *J. Geodesy* **1999**, *73*, 193–203.
47. Kandepu, P.; Foss, B.; Lamsland, L. Applying the unscented Kalman filter for nonlinear state estimation. *J. Process. Control.* **2008**, *18*, 753–768.
48. Xia, B.Z.; Chen, C.R.; Tian, Y.; Sun, W.; Xu, Z.H.; Zheng, W.W. A novel method for state of charge estimation of lithium-ion batteries using a nonlinear observer. *J. Power Sources* **2014**, *270*, 359–366.